Conjecture about the QCD phase diagram

José Antonio García-Hernández, Edgar López-Contreras, Elías Natanael Polanco-Euán and Wolfgang Bietenholz[*]

Instituto de Ciencias Nucleares, Universidad Nacional Autónoma de México
A.P. 70-543, C.P. 04510 Ciudad de México, Mexico
E-mail: joseantoniogarcia@ciencias.unam.mx, ed_lopez@ciencias.unam.mx,
elias.polanco@correo.nucleares.unam.mx, wolbi@nucleares.unam.mx

We present a phase diagram study of the O(4) model as an effective theory for 2-flavor QCD. In the chiral limit, both theories perform spontaneous symmetry breaking with isomorphic groups, which suggests that they belong to the same universality class. Since we are interested in high temperature, we further assume dimensional reduction to the 3d O(4) model, which implies topological sectors. According to Skyrme and others, the corresponding topological charge represents the baryon number. Hence the baryon chemical potential μ_B appears as an imaginary vacuum angle, which can be included in the lattice simulations without any sign problem. We present simulation results for the critical line in the chiral limit, and for the crossover in the presence of light quark masses. The shapes of these lines are compatible with other conjectures, but up to about $\mu_B \approx 300$ MeV we do not find a Critical Endpoint, although there are indications for it to be near-by.

---

[*]Speaker

1. The O(4) model as an effective theory for 2-flavor QCD

The QCD phase diagram is one of the most prominent open puzzles within the Standard Model. What we know quite well is the behavior at baryon chemical potential $\mu_B = 0$, which corresponds to zero baryon density.

• For massless quarks u and d, we expect a second order phase transition. If we add the s-quark with its physical mass, the critical temperature is around $T_c \simeq 132$ MeV [1]. For $2 + 1 + 1$ flavors, with $m_u = m_d = 0$ and physical masses m_s and m_c, the transition turns into a crossover, but the pseudo-critical temperature is practically the same, $T_{pc} \simeq 134$ MeV [2].

• In the case of physical quark masses m_u, m_d, m_s, lattice studies reveal again a crossover, now at a pseudo-critical temperature of $T_{pc} \simeq 155$ MeV, see *e.g.* Refs. [3]. This value of T_{pc} is compatible with the experimentally measured freeze-out temperature of the quark-gluon plasma.

At $\mu_B > 0$, lattice QCD is plagued by a notorious "sign problem" (see *e.g.* Ref. [4]), which prevents the exploration of the QCD phase diagram at finite baryon density. Despite numerous efforts, there is still no breakthrough in the attempts to overcome this sign problem. Therefore it is still appropriate to elaborate conjectures about the QCD phase diagram based on effective theories.

Here we consider the O(4) non-linear σ-model, which is assumed to be in the same universality class as 2-flavor QCD in the chiral limit [5]. Adding an external "magnetic field" (or "ordering field") $\vec{h}$ corresponds to a degenerate quark mass, and we obtain the Euclidean action

$$S[\vec{e}] = \int d^3x \int_0^\beta dx_4 \left[\frac{F_\pi^2}{2} \partial_\mu \vec{e}(x) \cdot \partial_\mu \vec{e}(x) - \vec{h} \cdot \vec{e}(x) \right], \quad \vec{e}(x) \in S^3, \ F_\pi \simeq 92.4 \text{ MeV} . \quad (1)$$

At $h = |\vec{h}| = 0$ the action has a global O(4) symmetry, which can break spontaneously to O(3). $h > 0$ adds some explicit symmetry breaking, in analogy to degenerate quark masses $m_u = m_d > 0$. There is a local isomorphy with or without symmetry breaking,

$$\{ \text{SU(2)}_L \otimes \text{SU(2)}_R \,\hat{=}\, \text{O(4)} \} \quad \longrightarrow \quad \{ \text{SU(2)}_{L=R} \,\hat{=}\, \text{O(3)} \} ,$$

which supports the assumption that the systems near criticality are in the same universality class.

We are interested in high temperature $T = 1/\beta$, so we assume dimensional reduction to the 3d O(4) model,

$$S[\vec{e}] = \beta \int d^3x \left[\frac{F_\pi^2}{2} \partial_i \vec{e}(x) \cdot \partial_i \vec{e}(x) - \vec{h} \cdot \vec{e}(x) \right] = \beta H[\vec{e}] . \quad (2)$$

We are going to consider cubic lattice volumes, $V = L^3$. With periodic boundary conditions, the configurations fall in topological sectors, $\pi_3(S^3) = \mathbb{Z}$. As pointed out by Skyrme and others, the topological charge Q corresponds to the baryon number B [6]. The field $\vec{e}(x)$ seems to represent just the pions, but its topological windings also account for baryons. Hence the baryon chemical potential μ_B corresponds to an imaginary vacuum angle θ, which extends the Hamilton function to $H[\vec{e}] = \cdots - \mu_B Q[\vec{e}] \in \mathbb{R}$.

2. Quark mass and chemical potential without sign problem

We are going to use the standard lattice action (in lattice units)

$$S_{lat}[\vec{e}] = -\beta_{lat} \left(\sum_{\langle xy \rangle} \vec{e}_x \cdot \vec{e}_y + \vec{h}_{lat} \cdot \sum_x \vec{e}_x + \mu_{B,lat} Q[\vec{e}] \right), \quad (3)$$

with $\beta_{\text{lat}} = \beta F_\pi^2$, $\vec{h}_{\text{lat}} = \vec{h}/F_\pi^2$, $\mu_{B,\text{lat}} = \mu_B/F_\pi^2$. For the topological charge of a lattice configuration, we employ the geometric definition, which assures $Q[\vec{e}] \in \mathbb{Z}$. We split each lattice unit cube into 6 tetrahedra, as illustrated in Figure 1 (left). The 4 spins attached to the vertices of one tetrahedron, say $(\vec{e}_w, \vec{e}_x, \vec{e}_y, \vec{e}_z)$, span a *spherical tetrahedron* on S^3, as symbolically sketched in Figure 1 (right): the edges $e_1 \ldots e_6$ are geodesics in S^3. The topological density of a tetrahedron is given by the oriented volume of this spherical tetrahedron, $V_{w,x,y,z}[\vec{e}] \in (-\pi^2, \pi^2)$, which is normalized such that

$$Q[\vec{e}] = \frac{1}{2\pi^2} \sum_{\langle wxyz \rangle} V_{w,x,y,z}[\vec{e}] \in \mathbb{Z} . \tag{4}$$
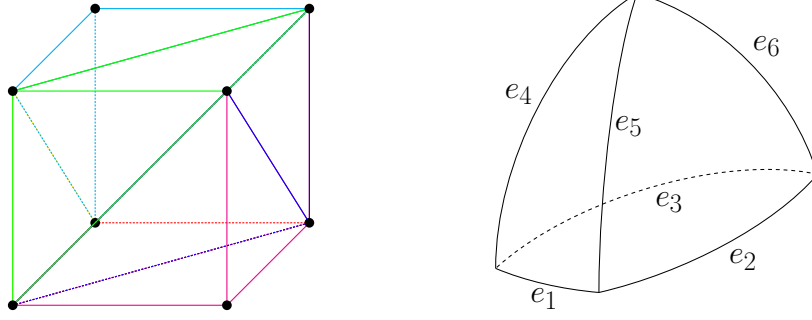

Figure 1: Left: division of a lattice unit cube into 6 tetrahedra. Right: symbolic sketch of a spherical tetrahedron on S^3. The topological charge is composed of the oriented volumes of such spherical tetrahedra.

We have implemented a rather involved, implicit formula for $V_{w,x,y,z}[\vec{e}]$, which was derived in Ref. [7]. However, it is computationally more efficient to choose some reference point on S^3 and count the tetrahedra which enclose this point, in an oriented sense. (We checked extensively that the results coincide.)

The applicability of an efficient cluster algorithm is another benefit of the O(4) model as an effective theory. We used the multi-cluster Wolff algorithm, which is particularly useful to avoid topological freezing. Different values of μ_B are taken into account by modifying the cluster flip probability, along the lines of Ref. [10]. As an example, Figure 2 shows the exponential auto-correlation time for the energy H, τ_H, and for the topological charge Q, τ_Q, in the lattice volume $V = 20^3$, at $h = 0$. They hardly differ, thanks to the cluster algorithm. Still, for increasing $\mu_{B,\text{lat}}$, τ rises rapidly: at $\mu_{B,\text{lat}} = 2.5$ it already exceeds 1000 multi-cluster sweeps, which has prevented us (so far) from exploring $\mu_{B,\text{lat}} > 2.5$. In all our data sets, the measurements were separated at least by 2τ; without being very careful, one can indeed be led to wrong conclusions about a Critical Endpoint (CEP). From Figure 2 we already suspect that we stay with a second order phase transition up to $\mu_{B,\text{lat}} = 2.5$, where τ would diverge in infinite volume at the critical value $\beta_{\text{c,lat}}$.

3. Conjectured phase diagram in the chiral limit

We first present our results at $h = 0$, *i.e.* in the chiral limit, where we deal with a second order phase transition, at least at low $\mu_{B,\text{lat}}$. We convert lattice units to physical units by referring to the critical temperature at $\mu_B = 0$. On the lattice, it was measured to high precision, $\beta_{\text{c,lat}} = 0.93590$ [9], which we match with the aforementioned lattice QCD result of $T_c \simeq 132$ MeV, such that

$$\mu_B = \frac{\beta_{\text{c,lat}}}{\beta_{\text{c}}} \mu_{B,\text{lat}} \approx 124 \text{ MeV } \mu_{B,\text{lat}} . \tag{5}$$
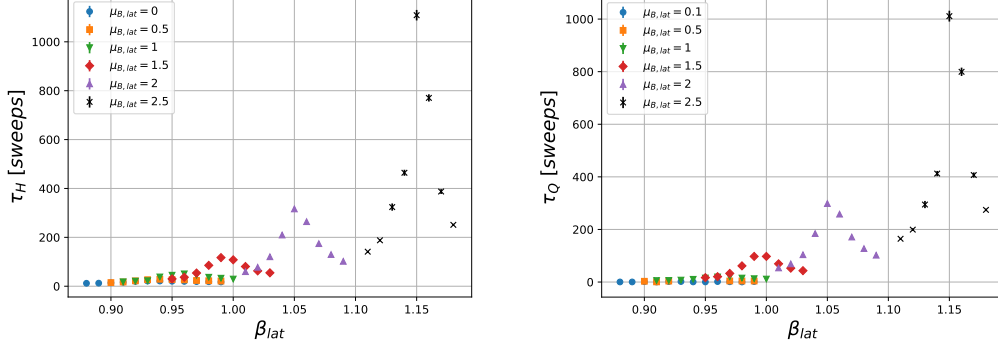
3

Figure 2: The auto-correlation time τ, in units of multi-cluster update sweeps, for the energy (τ_H) and the topological charge (τ_Q), which are very similar. These examples refer to $L = 20$, $h = 0$.

We simulated at $\mu_{B,\text{lat}} = 0$, 0.1, 0.2, ... 1.5, 2, 2.5, which corresponds to the range $\mu_B = 0 \ldots 309$ MeV. We are restricted to modest lattice volumes $V = L^3$, $L = 10$, 12, 16, 20, due to the problem with the huge auto-correlation time at our largest values of $\mu_{B,\text{lat}}$. For each parameter set, we performed 10^4 measurements, with perfectly thermalized and de-correlated configurations. In order to monitor the phase transition and its order, we measured some observables given by first and second derivatives of the free energy $F = -T \ln Z$ [8].

The plots in Figure 3 on top show the energy density $\epsilon = \langle H \rangle / V$ and the magnetization density $m = \langle |\vec{M}| \rangle / V$, $\vec{M} = \sum_x \vec{e}_x$ (the order parameter), which are first derivatives of F, at $L = 20$. We see that increasing $\mu_{B,\text{lat}}$ at fixed β_{lat} enhances ϵ but reduces m, as expected when more topological windings appear. In particular for our largest values of $\mu_{B,\text{lat}}$ we clearly see intervals of maximal slope, which coincide and move to larger β_{lat} when $\mu_{B,\text{lat}}$ increases. This indicates the approximate value of $\beta_{c,\text{lat}}$. At $\mu_{B,\text{lat}} = 2.5$ these slopes turn into quasi-jumps, so one might wonder whether a first order phase transition is near-by, or even attained.

The lower four plots in Figure 3 refer to second derivatives of F, namely the specific heat c_V and the magnetic susceptibility χ_m,

$$c_V = \frac{\beta_{\text{lat}}^2}{V}\left(\langle H^2 \rangle - \langle H \rangle^2\right), \quad \chi_m = \frac{\beta_{\text{lat}}}{V}\left(\langle \vec{M}^2 \rangle - \langle \vec{M} \rangle^2\right). \tag{6}$$

At $L = 20$ (plots on the left), we see pronounced peaks, in particular at $\mu_{B,\text{lat}} = 2$ and 2.5, hence the corresponding phase transition (in infinite volume) is likely to be still second order. Regarding the L-dependence at fixed $\mu_{B,\text{lat}}$ (plots on the right), the peak location of c_V hardly moves, but in the case of χ_m a thermodynamic extrapolation is important; it leads to values of $\beta_{c,\text{lat}}$, which are consistent with c_V and other criteria.

For a second order phase transition, the peak height of c_V is $\propto L^{\alpha/\nu}$; in the example of Figure 3 we obtain for the ratio of critical exponents $\alpha/\nu \approx 0.2$. The peak height of χ_m has a stronger L-dependence: in the range $\mu_{B,\text{lat}} = 0 \ldots 1.5$ we obtain $\gamma/\nu = 1.9(2)$, which is compatible with the precise result at $\mu_{B,\text{lat}} = 0$ from Ref. [9], $\gamma/\nu = 1.970$. Taking all that together strongly supports second order up to $\mu_{B,\text{lat}} = 2.5$.

Figure 4 (left) shows the topological charge density $q = \langle Q \rangle / V = \partial_{\mu_{B,\text{lat}}} F$, which vanishes at $\mu_{B,\text{lat}} = 0$ due to parity invariance. Topological winding is enhanced by $\mu_{B,\text{lat}} > 0$, but suppressed by low temperature. The plot on the right shows the topological susceptibility $\chi_t = (\langle Q^2 \rangle - \langle Q \rangle^2)/V$. Again we see pronounced peaks for $\mu_{B,\text{lat}} \geq 1.5$, at locations which agree with the previous determinations of β_c. If we use the peak height to define a ratio of critical exponents, in analogy to c_V and χ_m, $\chi_t(\beta_{c,\text{lat}}) \propto L^{x/\nu}$, we obtain e.g. $x/\nu|_{\mu_{B,\text{lat}}=0} \simeq 0.2$, $x/\nu|_{\mu_{B,\text{lat}}=1} \simeq 0.3$.
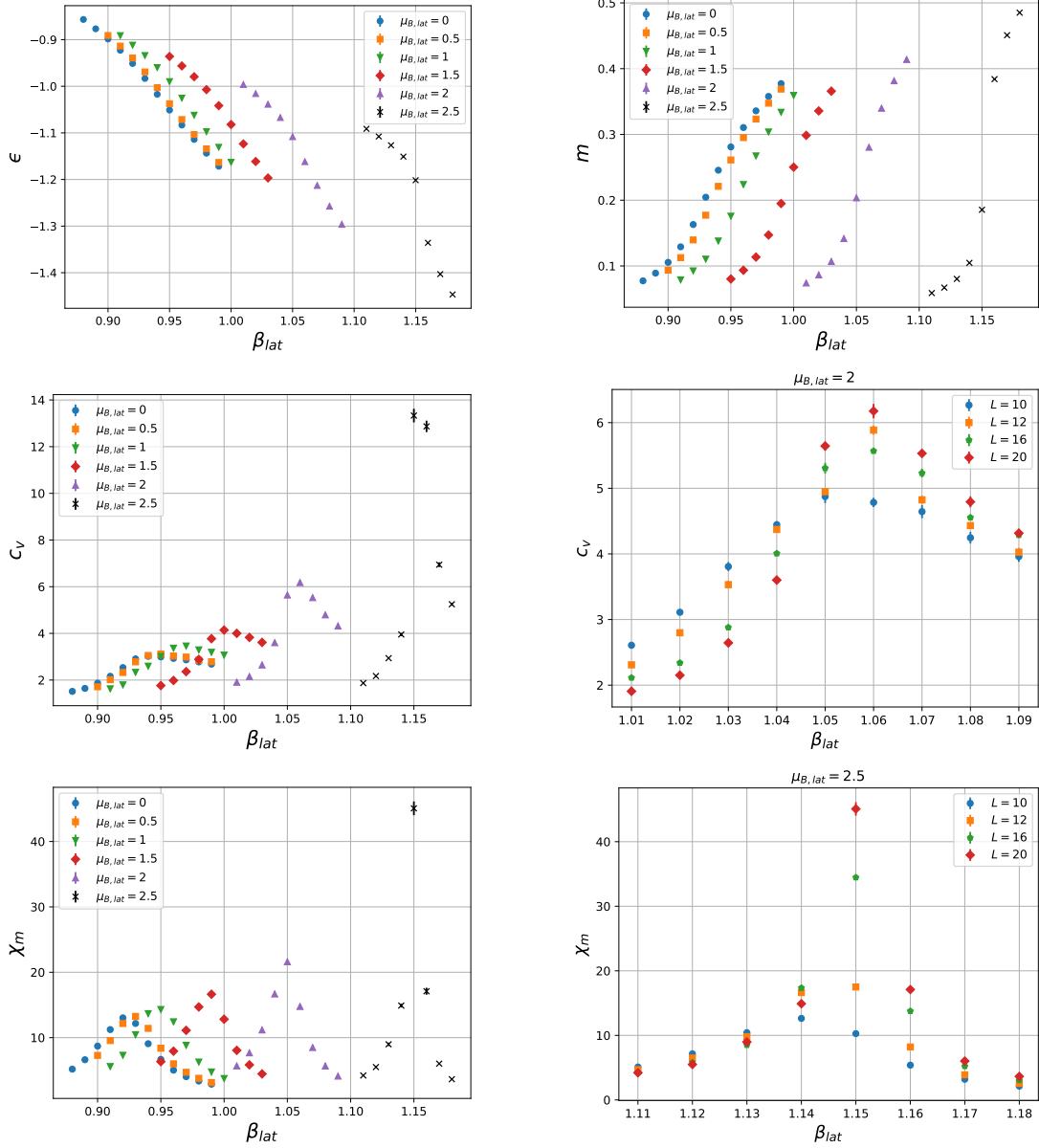
Figure 3: Simulation results at $h = 0$: energy density ϵ and magnetic density m (top), specific heat c_V and magnetic susceptibility χ_m (center and bottom). The β_{lat} interval where ϵ and m have maximal slopes agrees with the peaks of c_V and χ_m. We also show how the peak heights increase with the volume.
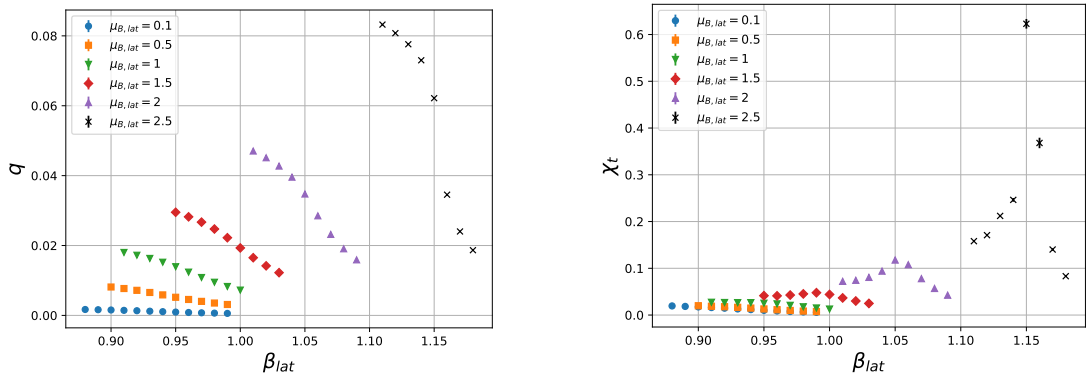

Figure 4: Topological charge density $q = \langle Q \rangle / V$ and the topological susceptibility χ_{t}, in the chiral limit.
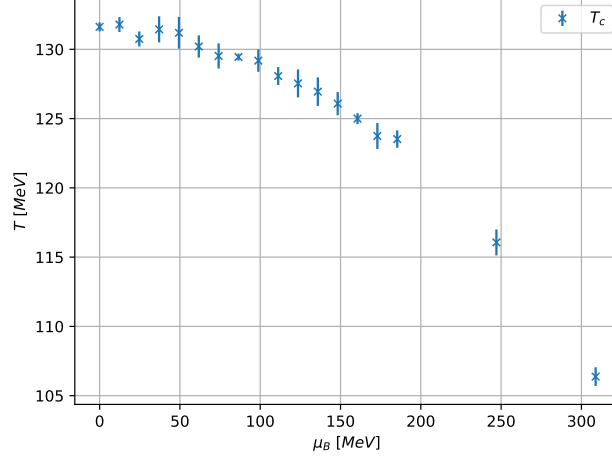
Figure 5: Conjectured phase diagram for QCD with 2 massless quark flavors.

Finally we combine all the determinations of $\beta_{\text{lat}}(\mu_{B,\text{lat}})$ (based on steepest slopes and peaks, also considering the correlation length, all extrapolated to $V \to \infty$), and convert to physical units. This leads to the phase diagram in the chiral limit shown in Figure 5. T_c decreases for increasing μ_B, in agreement with the consensus in the literature, but we do not observe a CEP (*i.e.* a change to a first order phase transition) in the regime $\mu_B \lesssim 309$ MeV and $T \gtrsim 106$ MeV.

4. Conjectured phase diagram with light quarks

We proceed to a finite, degenerate quark mass m_q of the light flavors u and d [11], which corresponds to the external magnetic field strength $h = |\vec{h}|$. In lattice units we choose the values $h_{\text{lat}} = 0.367$ and 0.14. Here we refer to the pseudo-critical crossover temperature $T_{\text{pc}} \simeq 155$ MeV to relate lattice units and physical units, $h \approx h_{\text{lat}} T_{\text{pc}}^4 / T_{\text{pc,lat}}^4$. Our results for $T_{\text{pc,lat}} = 1/\beta_{\text{pc,lat}}$ are ambiguous, as we see from the maxima of c_V and χ_m (see below). If we take the average, we obtain $T_{\text{pc,lat}}(h_{\text{lat}} = 0.367) \simeq 1.273$ and $T_{\text{pc,lat}}(h_{\text{lat}} = 0.14) \simeq 1.172$, in a monotonous relation to the chiral limit, $T_{\text{c,lat}}(h_{\text{lat}} = 0) = 1.06849$ [9]. For a dimensioned quantity like μ_B this suggests

$$\mu_B \approx 122 \text{ MeV} \, \mu_{B,\text{lat}} \quad (h_{\text{lat}} = 0.367) \, ; \qquad \mu_B \approx 132 \text{ MeV} \, \mu_{B,\text{lat}} \quad (h_{\text{lat}} = 0.14) \, . \tag{7}$$

If we interpret h as $m_q \Sigma$, and insert for the chiral condensate $\Sigma \simeq (250 \text{ MeV})^3$, we obtain the quark mass $m_q \approx 5.2$ MeV and $m_q \approx 2.7$ MeV, which is compatible with m_d and with m_u, respectively.

We incorporate the additional term by again adjusting the cluster flip probability, following Ref. [10]. We also implemented an alternative method, which adds a global "ghost field" with possible bonds to any spin variable [12].

Figure 6 shows results at $h = 0.367$: the auto-correlation time (top, left) is strongly alleviated thanks to the crossover; there is no critical slowing down anymore. The next three plots show the quantities ϵ, m and $\langle Q \rangle$ at various values of L, $\mu_{B,\text{lat}}$ and β_{lat}. ϵ depends somewhat on $\mu_{B,\text{lat}}$, but hardly on L, while for m some L-dependence is visible. These three observables are all smooth; there is no interval of a steep slope, in contrast to Figure 3. This is again consistent with the fact that the second order phase transition of the chiral limit is now washed out to a crossover.

For the same reason, c_V and χ_m do not exhibit actual peaks but rather smooth maxima, as we see in the lower two plots in the left column of Figure 6. We identify these maxima with Gaussian
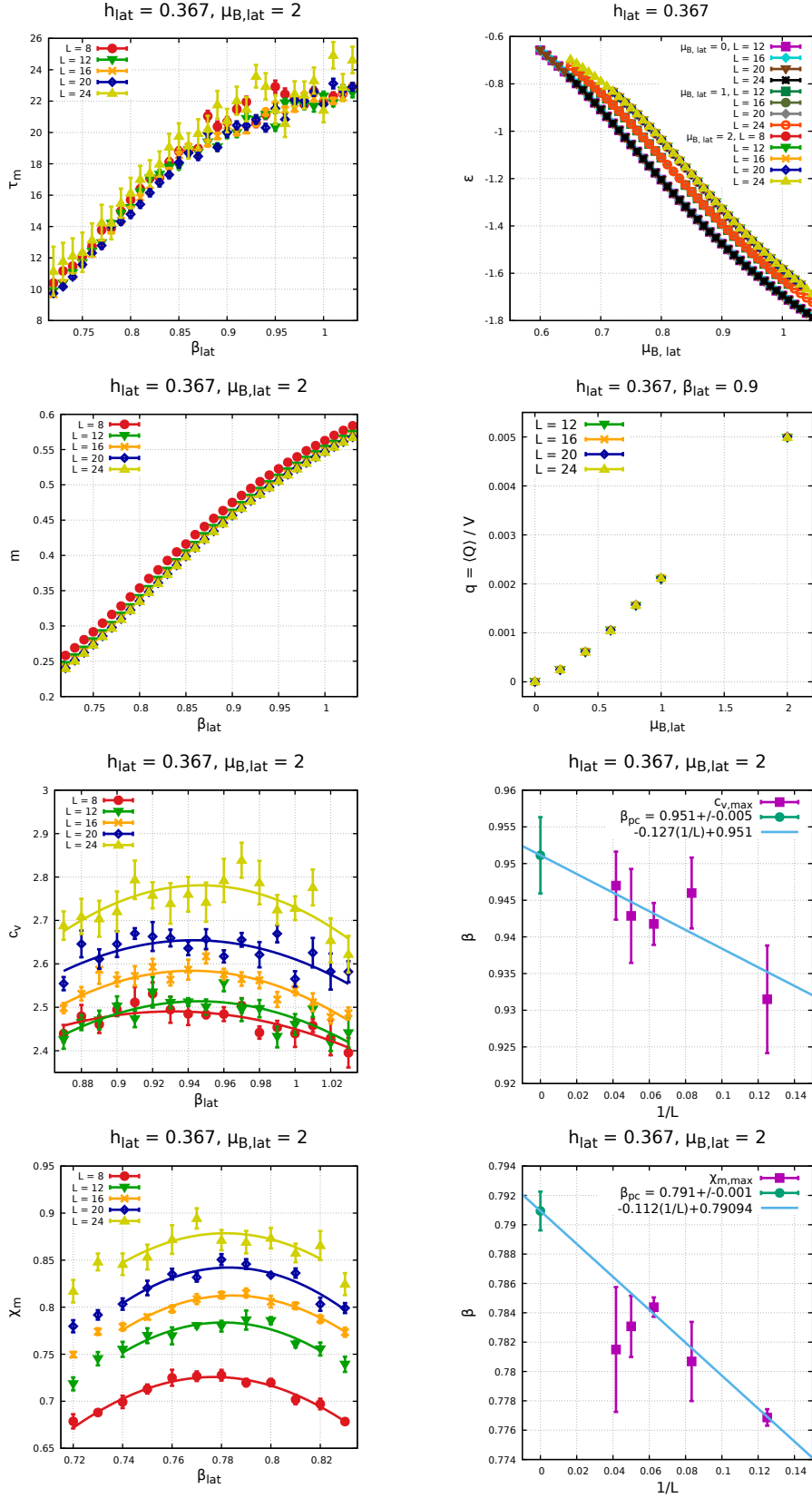
Figure 6: Simulation results of the effective theory at $h_{lat} = 0.367$, compatible with the quark mass m_d: τ_m as an example for the auto-correlation time; ϵ, m and $\langle Q \rangle$ as smooth first derivatives of the free energy F; c_V and χ_m with broad maxima, which we identify by Gaussian fits, and large-L extrapolations to $\beta_{pc,lat}$.
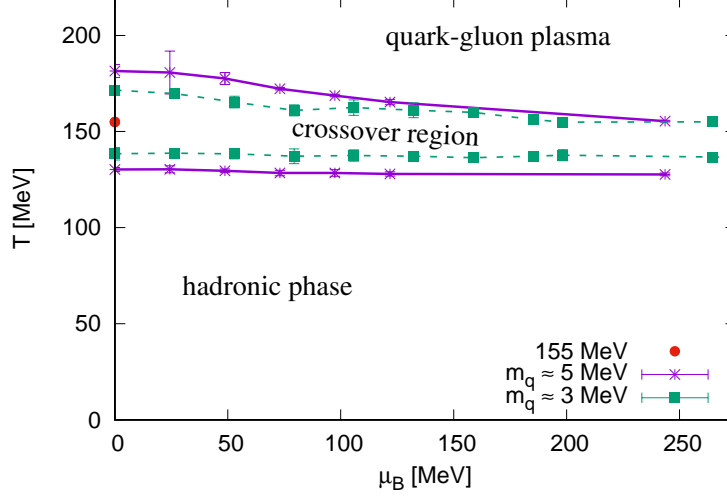
Figure 7: Conjectured phase diagram of 2-flavor QCD at $m_q \approx 5$ MeV, and at $m_q \approx 3$ MeV.

fits, and estimate their uncertainties with the jackknife method. The corresponding plots on the right illustrate the extrapolations to $\beta_{pc,lat}$ in the large-L limit.

Such extrapolations are performed at each $\mu_{B,lat}$-value, in order to monitor the crossover. There is a significant difference between extrapolated $\beta_{pc,lat}$-results obtained from c_V and from χ_m, which is again typical for a crossover. If we take them as the upper and lower bound of the crossover region, and convert to physical units as describe in the beginning of this section, then $T_{pc} \simeq 155$ MeV is in the center of the crossover interval at $\mu_B = 0$. Thus we arrive at the phase diagram in Figure 7, where we include the results obtained at $h = 0.14$, $L = 24$. We only see a slight trend for T_{pc} to decrease when μ_B increases, and there is again no indication of a CEP in the range that we explored, in this case up to $\mu_B \approx 250$ MeV.

5. Conclusions

We assume the O(4) model to be in the universality class of 2-flavor QCD in the chiral limit (O(N)-models cannot cope with more than 2 quark flavors). We refer to high temperature, which suggests a dimensional reduction to the 3d O(4) model, with a topological charge Q, which corresponds to the baryon number B. This effective theory can be simulated at finite baryon chemical potential μ_B, with a powerful cluster algorithm, and without any sign problem.

In the chiral limit, we monitored the critical line from $(\mu_B, T_c) \simeq (0, 132 \text{ Mev})$ to $(309 \text{ MeV}, 106 \text{ MeV})$. In this range, $T_c(\mu_B)$ decreases monotonically. No CEP is found, but there are hints for it to be near the endpoint of our study, so far.

If we add an external magnetic field, which roughly corresponds to the light quark masses, $T_{pc}(\mu_B)$ varies only little up to $\mu_B \approx 250$ MeV, and again there is no sign of a CEP. Figure 8 compares our bounds on T_{CEP} and $\mu_{B,CEP}$ to a multitude of other conjectures in the literature.
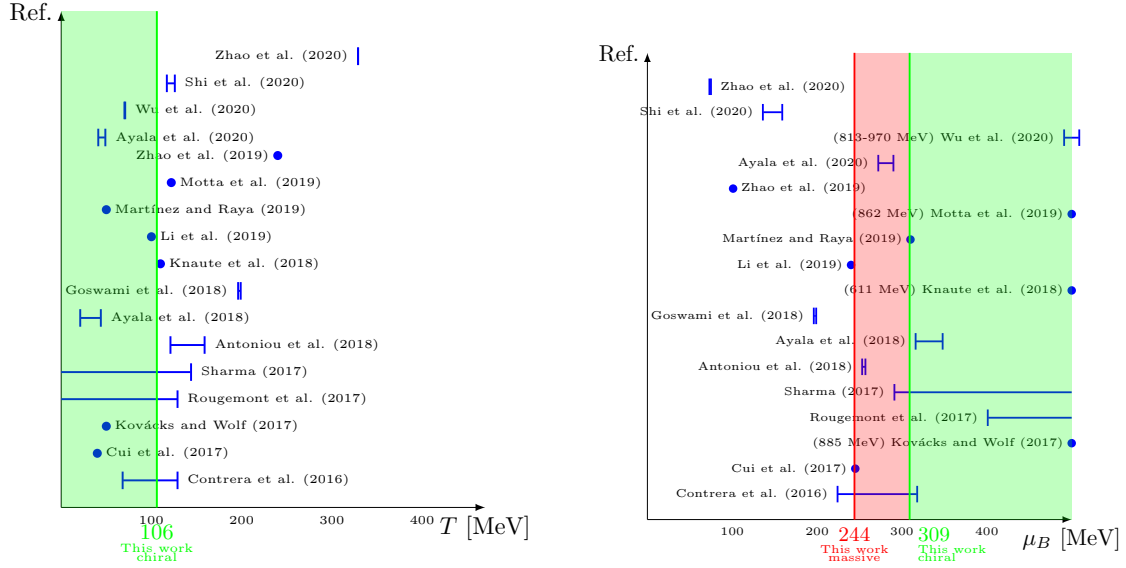
Figure 8: The allowed regions of T_{CEP} and $\mu_{B,CEP}$ as conjectured here, and in a number of other works.

References

[1] H.-T. Ding *et al.* (HotQCD Collaboration), Phys. Rev. Lett. 123 (2019) 062002.

[2] A.Yu. Kotov, M.P. Lombardo and A. Trunin, arXiv:2105.09842 [hep-lat].

[3] A. Bazavov *et al.* (HotQCD Collaboration), Phys. Lett. B 795 (2019) 15. T. Bhattacharya *et al.* (HotQCD Collaboration), Phys. Rev. Lett. 113 (2014) 082001.

[4] P. de Forcrand, PoS LAT2009 (2009) 010.

[5] R.D. Pisarski and F. Wilczek, Phys. Rev. D 29 (1984) 338. F. Wilczek, Int. J. Mod. Phys. A 7 (1992) 3911. K. Rajagopal and F. Wilczek, Nucl. Phys. B 399 (1993) 395. For a recent review, see A.Yu. Kotov, M.P. Lombardo and A. Trunin, Symmetry 13 (2021) 1833.

[6] T.H.R. Skyrme, Proc. Roy. Soc. Lond. A 260 (1961) 127; Nucl. Phys. (1962) 31 556. G.S. Adkins, C.R. Nappi and E. Witten, Nucl. Phys. B 228 (1983) 552. I. Zahed and G.E. Brown, Phys. Rept. 142 (1986) 1.

[7] J. Murakami, Proc. Amer. Math. Soc. 140 (2012) 3289.

[8] E. López-Contreras, B.Sc. thesis, Universidad Nacional Autónoma de México, 2021.

[9] M. Oevers, Diploma thesis, Universität Bielefeld, 1996. J. Engels, L. Fromme and M. Seniuch, Nucl. Phys. B 675 (2003) 533.

[10] J.-S. Wang, Physica A 161 (1989) 249.

[11] J.A. García-Hernández, B.Sc. thesis, Universidad Nacional Autónoma de México, 2020.

[12] C.M. Fortuin and P.W. Kasteleyn, Physica 57 (1972) 536. I. Dimitrović, P. Hasenfratz, J. Nager and F. Niedermayer, Nucl. Phys. B 350 (1991) 893.

[13] M.A. Nava Blanco, W. Bietenholz and A. Fernández Téllez, J. Phys. Conf. Ser. 912 (2017) 012048. M.A. Nava Blanco, M.Sc. thesis, Benemérita Universidad Autónoma de Puebla, 2019.